Phases Equilibrium Study in Quaternary Iron-rich Fe–Al–Mn–C Alloys

Vincent Rigaud, Dominique Daloz, Josée Drillet, Astride Perlade, Philippe Maugis, Gérard Lesoult

ISIJ International, Vol. 47 (2007), No. 6, pp. 898–906

Phases Equilibrium Study in Quaternary Iron-rich Fe–Al–Mn–C Alloys

Vincent RIGAUD,[1)] Dominique DALOZ,[1)] Josée DRILLET,[2)] Astrid PERLADE,[2)] Philippe MAUGIS[2,3)] and Gérard LESOULT[1)]

1) LSG2M UMR 7584 CNRS-INPL-UHP, Parc de Saurupt, F-54042 Nancy Cedex. E-mail: vincent.rigaud@mines.inpl-nancy.fr, dominique.daloz@mines.inpl-nancy.fr, gerard.lesoult@mines.inpl-nancy.fr 2) Arcelor Research, BP 30320, Voie Romaine, 57283 Maizières-lès-Metz, France. E-mail: josee.drillet@arcelor.com, astrid.perlade@arcelor.com
3) CIRIMAT CNRS-INPT, 118 route de Narbonne, 31077 Toulouse, France. E-mail: philippe.maugis@ensiacet.fr

(*Received on February 8, 2007; accepted on March 19, 2007*)

High aluminium low manganese steels were elaborated in order to study the phase equilibrium in the range of 900–1 100°C. Two different quaternary alloys have been studied (Fe–9 to 10wt%Al–1.7wt%Mn–0.2wt%C and Fe–9 to 10wt%Al–8wt%Mn–0.2wt%C). Equilibrium phase's nature was identified at four temperatures for two alloys. Equilibrium phase fraction and chemical compositions were determined at 900°C. Thanks to these equilibrium results, we tried to understand the non-equilibrium microstructure observed after different thermal histories (DTA cycles, isothermal treatment followed by quench, reception state) and identify DTA events in a coherent way.

KEY WORDS: iron; aluminium; manganese; carbon; phase transformation; quaternary alloys; iron aluminides.

1. Introduction

One approach to increase the specific properties of steel consists to add large aluminium content, allowing to reduce density: in that way, a 10% decrease of the density of steel could be achieved by alloying iron with 10 wt% aluminium, that is a low cost element, easily produced and which presents good corrosion and oxidation resistance.[1)] But these interesting properties are balanced by the improved sensitivity to environment and in particular hydrogen which weakens the alloy (leading to transgranular cleavage or intergranular cracking resulting from the penetration of hydrogen into the lattice). We can also mention the low ductility and impact resistance at low temperature and the low creep resistance at high temperature. All that points lead to delay commercial applications of iron aluminides.

In order to increase the intrinsic mechanical properties of the Fe–Al alloys, manganese and carbon additions seem promising candidates: on one hand, manganese and carbon stabilize the austenitic domain allowing to achieve an alpha/gamma phase transformation in the otherwise totally ferritic Fe–Al alloy.[2)] This allows to obtain α/γ duplex microstructure for manganese content less than 10 at%, which may lead to structural hardening and total stabilization of the austenite for manganese content above 10 at%, leading to TWIP or TRIP effects. On the other hand, by the ability to precipitate new carbides, called kappa, from which it is believed that structural hardening can be obtained. The kappa phase is a perovskite-type crystallographic structure with an ideal stoichiometry: Fe_3AlC. But exact composition of the kappa phase is hard to obtain, as explained by Palm *et al.*[3)]: "the solubility of carbon in iron–aluminum melts decreases rapidly with decreasing temperature leading to the precipitation of primary graphite… Therefore, single-phase material of the kappa-phase cannot be obtained directly from the melt." and: "Even after quenching one has to make sure that no change in composition and in phases equilibria take place during cooling to room temperature. This is especially crucial in case of the kappa phase: its homogeneity range is markedly shifted to higher C-concentrations with decreasing temperature". They estimate kappa composition as $Fe_{4-y}Al_yC_x$ ($0.8<x<1.2$ and $0.42<y<0.71$).[3)] But other authors describe it as Fe_3AlC_x.[4)] Precipitation of this carbide in quaternary Fe–Al–Mn–C alloys can occur from austenitic or ferritic matrix depending on the alloying element contents. Manganese atoms place in substitution on the iron atoms sites and transforms the stoichiometry of carbides to $(Fe, Mn)_3AlC_x$.

Until now, the main research works on quaternary alloys concern high manganese content alloys (>20 wt%) which present austenitic matrix. High manganese austenitic Fe–Mn–Al–C alloys are considered as strong alternatives to conventional stainless steels. Most of the studies on these alloys focus on the mechanical properties improvement by carbide precipitation[5–7)] or TWIP/TRIP effect development by manganese addition.[1,8–11)]

Ferritic matrix may also be interesting for mechanical properties if additional elements (C, Mn...) allow to precipitate new phases (γ or κ) enhancing matrix mechanical properties. This work concerns low manganese content quaternary alloys (2 to 10 wt%) which present ferritic matrix. This study aims to obtain multiphase microstructure

Table 1. Composition of the studied alloys.

Name	Fe (in wt%)	Al (in wt%)	Mn (in wt%)	C (in wt%)
Low Mn	Bal.	9-10	1.7	0.2
High Mn	Bal.	9-10	8	0.2

($\gamma/\kappa/\alpha$ or κ/α) and improve the understanding of phase transformation in this system, by estimating phase transformation temperature between 0 and 1 550°C and characterizing the microstructure for several heat treatments between 900 and 1 100°C.

2. Experimental Procedure

Table 1 gives the nominal composition of the alloys used in this study. The difference between these two alloys is their manganese contents and they will be referred as "low Mn" or "high Mn" alloys in the following text. In their reception states, the alloys were homogenised at 1 300°C during 45 min, hot rolled between 1 300 and 950°C and water quenched. Samples were elaborated by Arcelor Research in form of $150\times150\times5$ mm^3 sheets.

Figures 1 and **2** present the microstructure of the alloy in the reception state. Grains are oriented parallel to the rolling direction in both cases.

The "low Mn" alloy presents a three phases microstructure with globular precipitates (Fig. 2(A)) while the "high Mn" alloy seems to be a two phases microstructure with lamellar precipitates but consists of three phases (Fig. 2(B)). Transmission electron microscopy (TEM) analysis revealed that for the "low Mn" alloy, precipitates consist of kappa thin border and inner austenite while for the "high Mn" alloy, precipitates consist of austenite containing small ordered domains with a very thin border of kappa (less than 1 μm) represented by the small needles surrounding the inner austenite (Fig. 2(B)). Initial phase fractions of precipitates were measured: 16% for the "low Mn" alloy and 18% for the "high Mn" alloy.

First, differential thermal analyses (DTA) were performed to estimate phase transformation temperature in the range 0–1 550°C. These first experiments allowed us to choose an interesting temperature range to study phase's equilibrium by isothermal treatment. These were performed between 900 and 1 100°C. For DTA, the samples were cut from the initial sheet as small sticks with rectangular section of dimension $2.5\times2.5\times5$ mm^3. While for isothermal treatment, samples were prepared as $10\times10\times5$ mm^3 plates.

Differential thermal analysis treatments were performed on a SETARAM SETSYS 1750 DTA recorder that allows investigation up to 1 600°C. Each run is performed under argon gas flow, on a sample of ~150 mg placed in an alumina crucible, the reference is constituted of the same mass of alumina powder placed in another alumina crucible.

Two types of treatments have been achieved, the first one consists of a 0–1 550–0°C cycle for different heating and cooling speeds varying between 5 and 25 K/min (**Fig. 3**), the second one is a thermal treatment at fixed heat speed of 10 K/min until different maximal temperatures between 1 000 and 1 500°C were reached. Each cycle is performed twice to verify the data reproducibility. Due to the low confidence in the DTA signal for the low temperature domain, complementary measurements were performed between 0–800–0°C in a differential scanning calorimeter (SETARAM DSC 120) (Fig. 3). Samples were renewed between each experiment to maintain in each the same

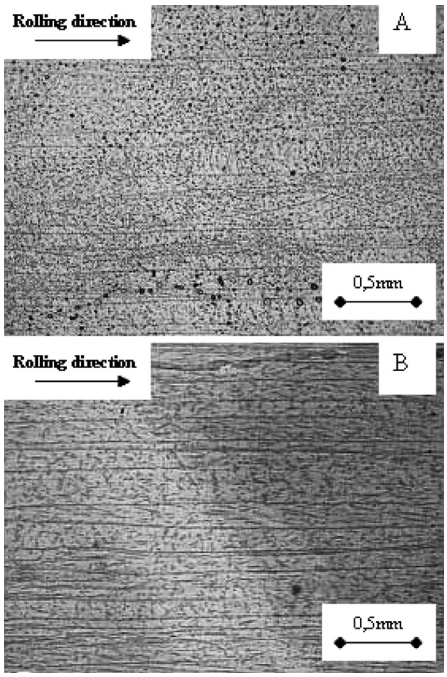

Fig. 1. Optical micrographs of samples in their reception state of the "low Mn" (A) and "high Mn" alloys (B) (Representing author=V. Rigaud).

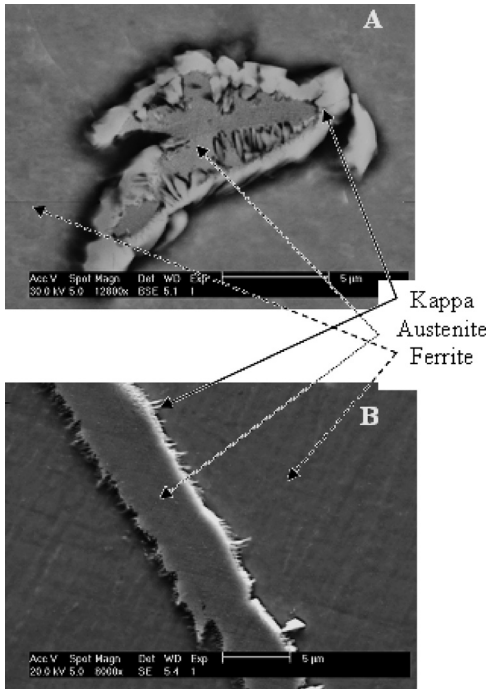

Fig. 2. MEB micrographs in secondary electrons which represent the multiphase microstructure of precipitate for the "low Mn" alloy (A) and the one phased structure for the "high Mn" alloy (B) (Representing author=V. Rigaud).

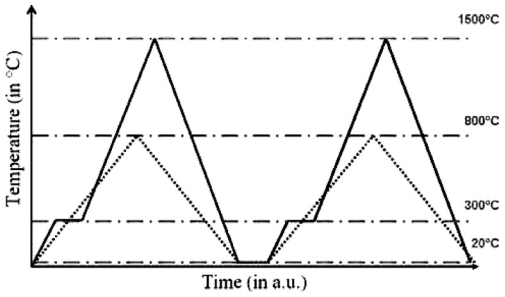

Fig. 3. DTA treatment performed between 0–800–0°C (dotted line) and 0–1550–0°C (full line) (Representing author = V. Rigaud).

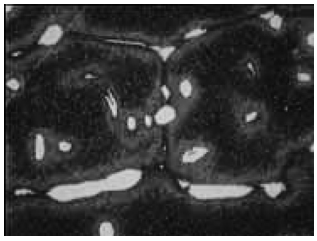

Fig. 4. Optical micrograph of modified Lepera etched sample. Kappa phase appears in white, while ferrite appears in dark. Colour shading in matrix is due to the reduced carbon content near grain boundary, acting as carbon trap (Representing author = V. Rigaud).

initial state.

Isothermal annealing treatments at 900, 1 000 and 1 100°C, from 15 min to 148 h for 900 and 1 000°C and from 15 min to 24 h at 1 100°C, followed by salted water quench were performed, completed by isothermal treatment at 1 000°C followed by slow furnace cooling under primary vacuum, with a cooling time of about 6–7 h. Microstructure observations were carried out by optical microscopy on Nital 4% etched samples and on a XL30 S-FEG SEM equipped with an EDX spectro-analyser. In addition, equilibrium phase's compositions were measured by WDS electron microprobe CAMECA SX 50. Phase fractions were measured by image analysis on optical microscopy image, using Aphélion® software, on modified Lepera etched samples. This modified etching solution consists of a first etching of 10 to 20 s with "100 mL water + 1 g sodium metabisulfide" mixed with "4 g picric acid + 100 mL ethanol", followed by a second etching of 10% sodium metabisulfide for a few seconds. Such etching was needed due to the high aluminium content of our alloys, leading to a thick alumina coating which is enough to prevent usual colouring etch solution to lay down sulphur coating on high carbon content area. Etching with disulfide allows to remove the protective alumina coating and to colour the sample (**Fig. 4**).

Transmission electron microscopy (TEM) investigations were performed in order to identify the phases nature. Electrolytic polishing of thin foils is a quick and reliable technique for TEM specimen preparation. However, in the case of Fe–Al–Mn–C steels, electrolytic polishing generates preferentially thinned ferrite grains and thicker kappa or austenite grains. To limit this problem, the most practical solution has consisted in minimising the electrolytic thinning time by reducing the specimen thickness to 20 μm by dimple grinding double face. The specimen perforation was performed using electrolytic polishing (solution composed of: 950 mL acetic acid + 50 perchloric acid, voltage: 70 V, temperature 16 to 18°C). The specimens were further ion milled (1 mA total current, 3.6 kV accelerating voltage, 10° incidence) for a maximum of 10 min to remove the surface oxide layers.

The both kappa and austenite have a FCC structure with a difference in lattice parameter too weak to be observed in diffraction patterns. However, in addition to the reflection spots of austenite, kappa phase exhibits some superlattice spots produced by the ordered microstructure. The identification of the kappa phase is based on the presence of these superlattice reflexions. **Figure 5** gives an example of diffraction pattern corresponding to the kappa phase.

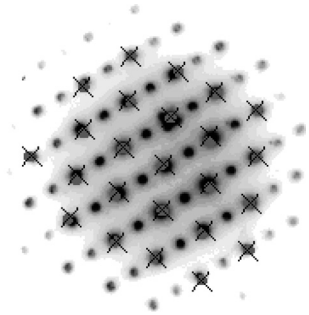

Fig. 5. Diffraction pattern of the kappa phase: zone axis [110]. A diffraction pattern of austenite in the same orientation only exhibits the crosses (Representing author = J. Drillet).

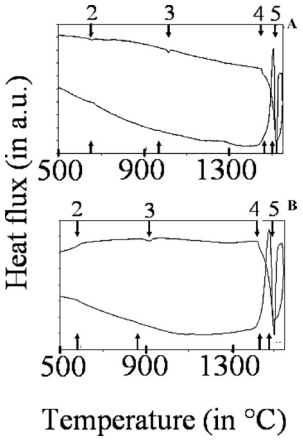

Fig. 6. Reversibility of DTA events during heating and cooling for the "low Mn" (A) and the "high Mn" (B) alloys (Representing author = V. Rigaud).

3. Results

3.1. Differential Thermal Analysis: Phase Transformation Temperature

Characteristic thermal analysis data are presented in **Fig. 6**. The main events attributed to phase transformations are reversible; each event occurs in the heating cycle and has its symmetric in the cooling cycle.

Each event was defined by three temperatures (peak start/peak maximum/peak end). Here we just give the average event maximum temperature for all the samples studied. The start and end temperature of events does not ap-

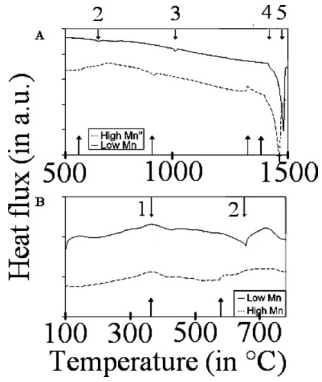

Fig. 7. Characteristic DTA (A) and DSC (B) curves for the "low Mn alloy" and the "high Mn alloy" during heating (Representing author＝V. Rigaud).

Table 2. Events identified as phase transformations for the two alloys by DTA.

Mn content	Event 1	Event 2	Event 3	Event 4	Event 5	Event 6
Low Mn	~300°C	-	660°C	1020°C	1450°C	1520°C
High Mn	~300°C	575°C	920°C	1200 - 1400°C	1420°C	1510°C

pear due to the strong dependence of these temperatures to the heating and cooling speeds and the definition of the baseline. Events are defined as part of the curve presenting at least one slope change more or less pronounced (**Figs. 7**(A) and 7(B)).

The different reversible events identified are presented in **Table 2** (±10°C). The same events are present in the two alloys except the event 2, which is only present in the "high Mn" alloy. The events 1 to 4 are not very intense comparing to events 5 and 6. One hypothesis to explain this could be the low corresponding phase fraction of second phase precipitate and strong spreading over a large range of temperature, in particular for event 4. Comparing the two alloys thermograms illustrate the effect of the manganese content on transformation temperature in solid state. The more the alloy contains manganese, the more the transformation temperatures are shifted to higher temperatures. Metallographic analysis should give more information on the different phase fields.

The continuity between the two types of experiments is good, as can be seen on observing the event 2 (see Table 2). The following table gives the corresponding temperature of the different events identified by differential thermal analysis. Events 5 and 6 were identified as solidus and liquidus due to their characteristic shape. Temperatures presented in Table 2 are average temperatures for heating and cooling cycle.

Table 3 presents average temperatures for solidus and liquidus for the different cycles. Temperatures are lower for the cooling cycle due to the microsegregation of slow diffusing elements during solidification step.

To summarize, DTA experiments allowed us to note the presence of some events for which we associated estimated temperatures (Table 2). We also determined an average value for the liquidus and solidus temperature of the two alloys.

Table 3. Average temperature for solidus and liquidus for the different thermal cycles of the two alloys.

Mn content	Solidus (Heating / Cooling)	Liquidus (Heating / Cooling)
Low Mn	1460 / 1445°C	1540 / 1520°C
High Mn	1435 / 1490°C	1520 / 1515°C

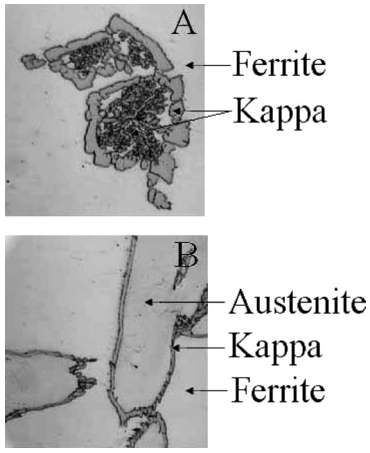

Fig. 8. Optical micrographs of "low Mn alloy" (A) and "high Mn alloy" (B) after two thermal analysis cycles up to 1 550°C (10 K/min) (Representing author＝V. Rigaud).

Table 4. Phase fraction constituting precipitates after DTA treatment at 1 550°C with a heating and cooling rate of 10 K/min.

Phase	Low Mn	High Mn
Kappa	~10%	a few percent
Austenite	0%	~20%

3.2. Differential Thermal Analysis: Microstructural Analysis

3.2.1. As Solidified State

Two different microstructures are observed depending on the manganese content for a cooling speed of 10 K/min (**Fig. 8**). For the "low Mn" alloy, the microstructure consists of two phases with a ferritic matrix and κ phase precipitates. These precipitates present a ring-like structure from which the border of the ring consists of homogeneous kappa phase while the inner part consists of small globular kappa precipitates and ferrite with modified alloying element contents (Fig. 8(A)).

For the "high Mn" alloy, the microstructure is composed of three phases: the ferritic matrix, kappa precipitates and the austenitic phase. In such alloy, the kappa precipitate surrounds as a thin border (from 1 to 5 μm thick) the thick homogeneous austenitic phase (from 20 to 10 μm thick) (Fig. 8(B)).

In order to determine the solid state transformation path which leads to the microstructure presented on Fig. 8, and to identify the events obtained by DTA, we decided to compare the microstructure of our two alloys obtained after one DTA cycle (melting and solidification). **Table 4** gives the phase fractions of precipitates in the matrix after DTA treatment at 1 550°C. These precipitates were identified as kappa phase for the "low Mn" alloy and $\kappa+\gamma$ for the "high Mn" alloy by EDX analysis. The phase fractions indicated

for kappa in the "high Mn" alloy is not accurate due to the fact that our image analysis software does not discern the kappa ring-like structure and the inner globular austenite precipitates (Fig. 8).

DTA as solidified microstructure analysis shows two different kinds of precipitates depending on the manganese content of the alloy. "Low Mn" alloy presents about 10% of kappa globular precipitates, while the "high Mn" alloy presents about 20% of lamellar precipitates consisting of austenite with a thin border of kappa phase.

3.2.2. Microstructure after Thermal Cycling

Figure 9 presents the typical microstructure observed in both alloys, after different 20°C–*X*°C–20°C DTA runs realised on sample in reception state at a heating and cooling rate of 10 K/min (with *X* varying between 1 000 to 1 500°C by steps of 100°C).

Two distinct microstructures can be observed depending on the maximum temperature reached during the thermal treatments:

– When the maximum temperature of the treatment exceeds 1 200°C, the microstructure obtained is identical to the as solidified one, previously described (compare Fig. 9(A)–(B) and Fig. 8(A)–(B)).
– When the maximum treatment temperature is lower than 1 100°C, a different microstructure is observed. For the "low Mn" alloy, the microstructure is composed of $\alpha+\kappa$ phases, with kappa globular precipitates forming aggregates inside the matrix (Fig. 9(C)). For the "high Mn" alloy, the microstructure is also consisting of two phases, the kappa phase changes from the thin border structure to the "ring-like" type presented for the as solidified state. In this latter case, inner austenitic phase of precipitates observed at high temperature disappeared (Fig. 9(D)).

To summarize, we obtain the same kind of microstructures for the two alloys, consisting of ferritic matrix and kappa precipitates, after different DTA cycling with maximum temperature under 1 100°C. While the microstructure are identical to the one observed for each alloy in the as solidified state, after different DTA cycling with maximum temperature above 1 200°C.

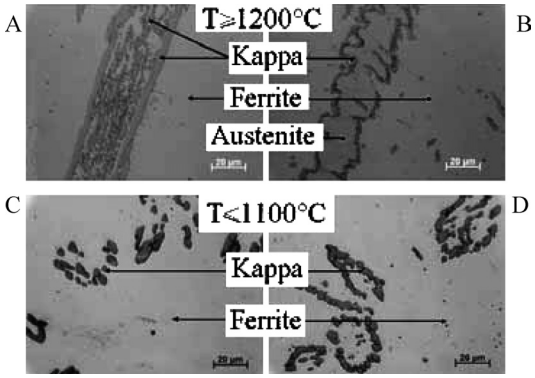

Fig. 9. Optical micrograph of "low Mn alloy" (A and C) and of "high Mn alloys" (B and D) after two thermal analysis cycles up to 1 500°C at 10 K/min (Magnification ×500). A and B are representative of treatments performed above 1 200°C, while C and D are representative for treatments under 1 100°C (Representing author=V. Rigaud).

3.3. Thermal Treatment: Microstructure Analysis

3.3.1. Isothermal Holding

Isothermal treatments followed by water quench were performed from 900 to 1 100°C. First, these treatments allowed us to characterize the microstructures of the alloys at these temperatures and their formation kinetics represented by their phase fraction evolution with treatment time. Next, it gives us information related to phase equilibrium at these temperatures.

Typical microstructures are presented in **Fig. 10**, corresponding to 30 min annealing at different temperatures. All the samples exhibit a ferritic matrix. The "low Mn" alloy presents kappa precipitates (Fig. 10(A)), while the "high Mn" alloy presents mainly austenitic precipitates (Fig. 10(B)), as identified *via* TEM (**Figs. 11** and **12**).

In Fig. 10(B), we observe mainly austenite in precipitates but we can suppose the presence of a very thin kappa border by continuity with previous observations, which were not characterized precisely.

The analysis of these micrographs illustrates that it appears an acicular structure during the quench. These structures correspond to a quench phase. Literature suggests that it can correspond to three different phases: 18R martensite, austenite or kappa.[6,12–14] 18R martensite can be excluded from the conceivable precipitating phases due to the fact

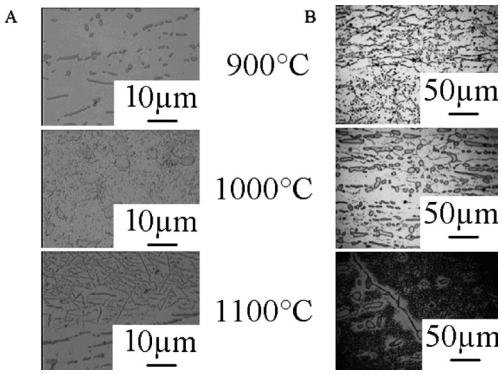

Fig. 10. Optical micrograph of sample from the two alloys after isothermal annealing during 30 min at different temperatures followed by salted water quench for the "low Mn alloy" (A) and the "high Mn alloy" (B). Magnifications are different to make satisfactory observations on each alloy (Representing author=V. Rigaud).

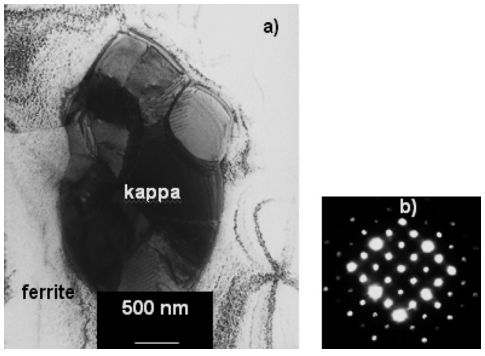

Fig. 11. Low Mn content. Sample quench after 30 min of holding at 900°C. TEM micrograph (a) and diffraction pattern (b). Kappa: zone axis [001] (Representing author=J. Drillet).

that they appear under the form of ~100 μm long plates in samples quenched from above 1 300°C.[6,12] The precipitation of this quenched structure enlightens a needle free area around the precipitates. The precipitates in the two alloys present high carbon contents, draining all the carbon of the surrounding matrix, which explains the needle free zone around them. The reader should imagine the same microstructures without the needles to have an idea of what they should look like at high temperature.

Figure 13 presents phase fraction evolution with treatment time. We can conclude that phase fraction decrease with increasing treatment time at these temperatures. We consider that equilibrium is achieved when the phase fraction does not change anymore with treatment time. As the alloy is enough isotropic, we consider that measured surface phase fractions are representative of volume fractions.

Table 5 presents the phase fraction at equilibrium. The following statements can be made:

– At 900°C, the equilibrium is obtained after 8 h of treatment for the "high Mn" alloy, while the volume fraction of second phase still decreases after 24 h of treatment for the "low Mn" alloy. In both cases, the equilibrium structure is composed of two phases: α and κ.
– For treatment performed at 1 000°C, 1 h of annealing treatment is sufficient to stabilize the "high Mn" alloy in a $\alpha+\gamma$ microstructure while the "low Mn" alloy equilibrium is single phase a after 24 h of annealing.
– At 1 100°C, stabilization of the equilibrium $\alpha+\gamma$ structure is reached in less than 15 min for the "high Mn" alloy, as well as the total dissolution of kappa for the "low Mn" alloy.

The decrease of the austenitic precipitates fraction with the increase of temperature shows that the equilibrium should be fully ferritic at temperatures far above 1 100°C. The manganese content in "high Mn" alloy is responsible of the austenite phase fraction stabilization at lower temperature (Fig. 13).

We also measured particles size by image analysis at 900 and 1 000°C (**Fig. 14**). The radius increases with treatment time, which is characteristic of coarsening mechanisms. But the chemical composition has no strong effect on it as can be seen from Fig. 13 and **Table 6**.

The coarsening kinetics coefficient a of the precipitates,

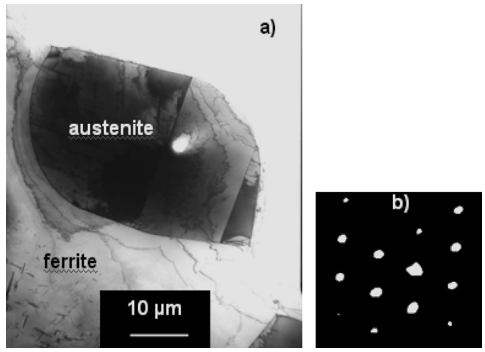

Fig. 12. High Mn content. Sample quench after 24 h of holding at 1 000°C. TEM micrograph (a) and diffraction pattern (b). Austenite: zone axis [110] (Representing author=J. Drillet).

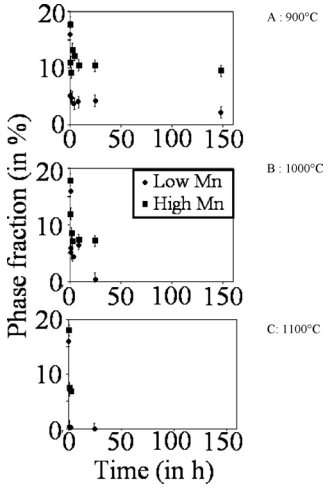

Fig. 13. Phase fraction evolution with treatment time at different temperatures (A: 900°C, B: 1 000°C and C: 1 100°C) (Representing author=V. Rigaud).

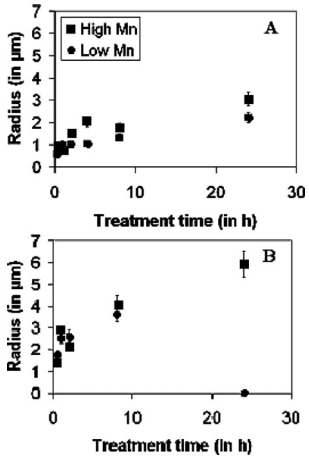

Fig. 14. Radius evolution of particles in function of treatment time (A: 900°C, B: 1 000°C) (Representing author=V. Rigaud).

Table 5. Precipitate phase fraction at equilibrium between 900 and 1 100°C.

	Volume fraction of precipitate phase at equilibrium (in %)	
	"Low Mn" alloy = κ precipitate	"High Mn" alloy = γ precipitate
900°C	~ 2	~ 9
1000°C	~ 0	~ 7
1100°C	~ 0	~ 7

Table 6. Value of the proportionality coefficient $\alpha=(3D\sigma N_{\alpha}V_m/2RT)$ as a function of the maximum temperature of treatment depending on the manganese content.

	900°C	1000°C
« Low Mn »	0.06	0.21
« High Mn »	0.08	0.17

determined from the measurements of the volume fractions in accordance to Greenwood's law: $r^3 - r_0^3 = \alpha \cdot t$[15] is reported in Table 6.

3.3.2. Slow Furnace Cooling

Slow furnace cooled samples from 1 000°C were analysed in order to investigate the effects of the cooling rate on the microstructure evolution. The results are presented in **Figs. 15** and **16**.

For the "low Mn" alloy, the two samples present an $\alpha + \kappa$ microstructure with more or less globular precipitates. For higher cooling speed, precipitates are thicker and the corresponding phase fraction is higher. This observation suggests that this phase is not kappa, but could be austenite. Kappa is a stoichiometric compound, for which stoichiometric deviations are not enough important to cause phase fraction modifications. Precipitate distribution in the alloy is more homogeneous for slow cooling speed, the precipitates begin to form aggregates for the higher cooling speed.

For the "high Mn" alloy, precipitates show ring like microstructure and are homogeneously distributed. For the slow cooling speed, precipitates consist of inner austenite with continuous kappa ring around it, which remind the microstructure observed for high temperature DTA experiments (maximum treatment temperature above 1 200°C). While it consists of kappa phase lonely for higher cooling speed. The kappa phase fraction seems identical for the two cooling speeds but the precipitates size increases, while the austenite disappeared for faster cooling.

From the same initial state, the same maximum treatment temperature and the same holding time, increasing cooling speed increases precipitates size but influence austenite transformation. Precipitates distribution may also be influenced by the cooling speed.

3.4. Microprobe Analysis

Microprobe analyses were performed to enhance our knowledge on phase's equilibrium. Measurements of iron, aluminium and manganese contents have been performed by electron probe analysis on the different phases of the alloys after 148 h of annealing at 900°C followed by quench (**Fig. 17**).

Figure 17 shows horizontal content profiles for all the elements in the different phases. This illustrates the fact that there is no concentration gradient at the microprobe scale, but TEM experiments revealed that such gradients exist at 100 nm scale. This means that equilibrium is not completely reached for this isothermal treatment time at 900°C, despite the results of the phase fraction analysis. Matrix and precipitates composition are homogeneous.

For the "low Mn" alloy, the κ phase presents an aluminium content of about 11.1 wt%, which is far from the admitted stoichiometric value for κ and higher than the matrix one. It also presents higher manganese and calculated carbons contents than the matrix ones.

Austenitic precipitates of the "high Mn alloy" show aluminium content of about 7.5 wt%, which shows that aluminium has a strong α-like effect and is essentially present in the matrix. The manganese and calculated carbon contents of austenitic precipitate are higher than the matrix ones, which is characteristic of the strong γ-like nature of these elements.

From the aluminium and manganese content profiles, it can be concluded which is the phase studied, but carbon content analysis would provide better information on the κ

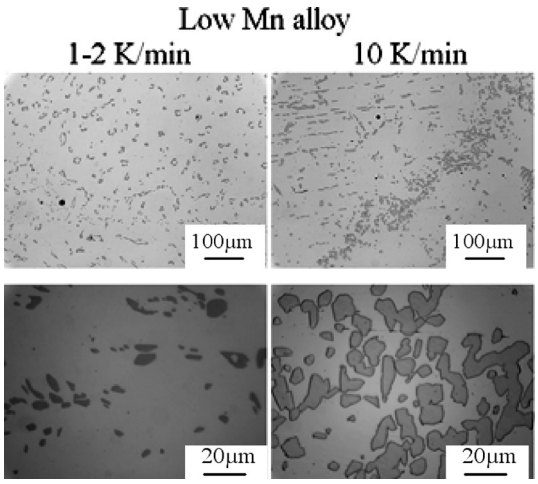

Fig. 15. Optical micrograph of a sample heated and held 15 min at 1 000°C and cooled at different speeds (Representing author = V. Rigaud).

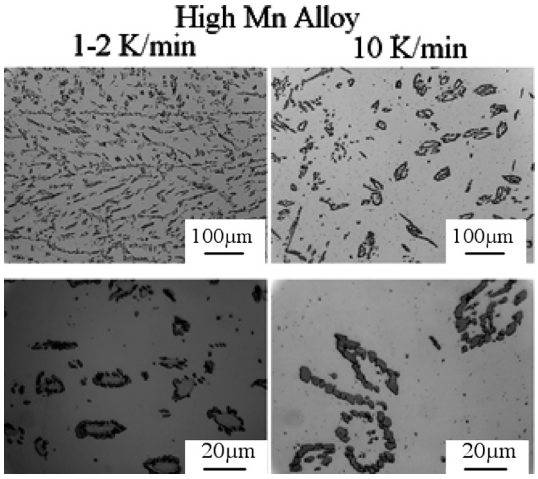

Fig. 16. Optical micrograph of a sample heated and held 15 min at 1 000°C and cooled at different speeds (Representing author = V. Rigaud).

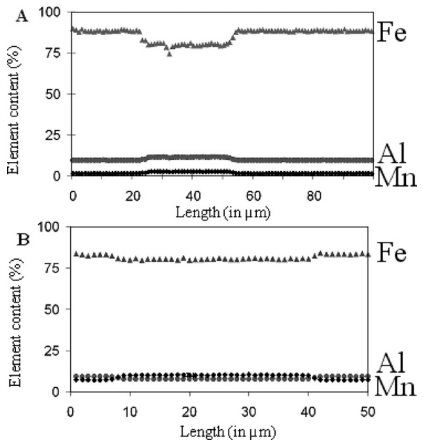

Fig. 17. Al and Mn content in wt% for the two alloys after annealing during 148 h at 900°C (A: "low Mn alloy" and B: "high Mn alloy") (Representing author = V. Rigaud).

Table 7. Equilibrium content of alloying elements in the different phases of our two alloys at 900°C.

Element	Low Mn		High Mn	
	Matrix content (in wt%)	Precipitate content (in wt%)	Matrix content (in wt%)	Precipitate content (in wt%)
Fe	88.4	80.5	82.9	80.00
Al	9.4	11.1	9.1	7.8
Mn	1.5	2.5	7.2	10.2
C (estimated)	<1	0<x<6	<1	0<x<2

phase's stoichiometry.

Table 7 gives the equilibrium concentrations calculated as an average of the elements content for the different phases of the two alloys. Carbon contents were calculated by subtracting average iron, aluminium and manganese contents from 100%, considering that it should be the main element remaining. It must not be taken as quantitative value but as information on the variation direction.

These microprobe analyses give us one tie-line of the quaternary equilibrium phase diagram at 900°C. The manganese and aluminium contents are higher in the kappa phase than in the ferritic matrix for the "low Mn" alloy. The manganese content is higher in the austenitic phase than in the ferritic matrix for the "high Mn" alloy, while the aluminium content is lower than the matrix one.

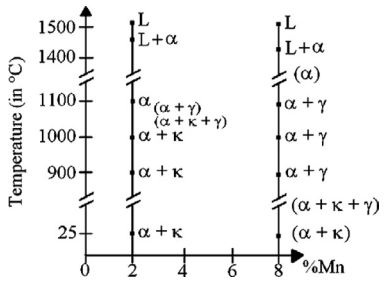

Fig. 18. Schematic isopleth section of quaternary Fe–Al–Mn–C system with C and Al content fixed, in which equilibrium results are represented in black and in parenthesis the other phase fields according to the following discussion (Representing author＝V. Rigaud).

4. Discussion

This section will try to describe which are the solid state transformation paths involved in the microstructure formation for the two alloys studied. We will explain the observed DTA events with our metallographic and phase nature analyses.

4.1. DTA Analysis

4.1.1. Low Mn

From our heating experiments, the first particle of ferrite appears in the liquid at ~1 540°C. The last droplet of liquid disappears at ~1 460°C, as stated by Table 2. Table 4 represents phase fraction evolution, it shows that the precipitation occurs between 1 100 and 900°C during cooling. At this point, we need to make the hypothesis that austenite should appear in the samples to be in agreement with the observations made on the initial hot rolled state. Metallographic observations do not allow concluding on the nature of the event 4, but considering the previous hypothesis, we can suppose that it must exist an $\alpha+\gamma$ domain. This can be related to event 4 of DTA analysis. Equilibrium experiments allow us to note that at 900°C, stable equilibrium phases are $\alpha+\kappa$, while above 1 100°C, it is α only. This kappa precipitation can be related to event 3 observed in DTA experiments, as confirmed by DRX analysis. The remaining event 1 at 300°C, which is more intense during cooling, and exhibits a lambda-like shape that can be attributed to the para-/ferro-magnetic transition.[1] This transition is also strongly affected by additional elements.[16,17]

4.1.2. High Mn

Starting from liquid state, the first solid ferrite particles will appear from liquid since 1 520°C and a fully solid state is reached at 1 435°C. Equilibrium experiments allow us to note that equilibrium consists of two phases $\alpha+\gamma$ at 900, 1 000 and 1 100°C. The phase fraction of austenite decreases with increasing temperature. Comparing this equilibrium results with the DTA results allow us to assimilate the event 4, extended between 800 and 1 400°C, with the formation of austenite which is due to the high manganese content which stabilizes the corresponding phase field to lower temperature than the one for the "low Mn" alloy. DTA event 3 corresponds to kappa precipitation as for "low Mn" alloy. The shift between the two alloys phase transformation temperature can be attributed to the grain boundaries acting as carbon traps, which leads to out of equilibrium structure. Event 2 can be attributed to spinodal decomposition of austenite into kappa phase, as stated by literature.[18,19] The event 1 should correspond to the magnetic transition due to the shape of the event.

4.2. Phase Equilibrium

Figure 18 shows a schematic isopleth section of the quarternary Fe–Al–Mn–C system with carbon and aluminium content fixed, in which equilibrium results are represented in black and in parenthesis the other phase fields according to the following discussion.

4.2.1. Low Mn

Low temperature stable equilibrium state consists of two phases $\alpha+\kappa$ (up to 900°C). While it consists only of one phase α for higher temperatures (more than 1 000°C), kappa disappears with increasing temperature because kappa phase is the stable precipitate for low temperature.

The kappa ring-like structure can be attributed to the remains of the reception state which is a non equilibrium state but comes from thermomechanical treatments (hot rolling). It presents the same kind of ring-like structure with inner austenite homogeneous phase. Hot rolling increased the grain boundaries area. Austenite precipitated on these large grain boundaries, which act as carbon traps, making austenite precipitation easier. Austenite must have transformed next into plenty of small globular inner precipitates of kappa phase in a modified ferritic matrix during

isothermal treatment, as observed in our metallographic experiments. At some time, it must have existed a two phase structure $\alpha+\gamma$, followed by a three phase structure $\alpha+\kappa+\gamma$. This three phase structure should have consisted of a ferritic matrix, presenting multiphase precipitates. These precipitates consist of inner austenite embedded by thinner kappa phase. The inner austenite phase transforms into a mix of kappa precipitates with depleted/enriched ferritic matrix during cooling. The corresponding fraction of inner phase should have been so high that the cooling time was not enough to allow the remaining kappa precipitates to coarsen.

From our results, we can suppose that austenite should appear for temperature between 900 and 1 000°C, leading to $\alpha+\kappa+\gamma$ and $\alpha+\gamma$ phase fields. These phase fields should appear just under the identified single phase ferritic field starting between 1 000 and 1 100°C. The produced austenite at grain boundaries formed in non equilibrium conditions.

4.2.2. High Mn

Phase equilibrium consists of two phases $\alpha+\gamma$ between 900 and 1 100°C. On cooling from high temperature, the austenite, stabilized at high temperature, will start to dissolve leading to a three phase structure $\alpha+\kappa+\gamma$, then leading to $\alpha+\kappa$ phase field, when decreasing temperature under 800°C.

The evolution of the austenite phase fraction with isothermal treatment temperature allow us to suppose that there will be a single phase domain above the $\alpha+\gamma$ phase field. This domain should appear for temperature above 1 100°C. Experiments showed that the low temperature austenitic domain stabilisation is linked to the manganese and carbon contents, which are potent austenite stabilizers while aluminium content is a ferrite stabilizer.

5. Summary

This study is a step forward to the understanding of solid state transformation in low manganese content Fe–Al–Mn–C alloys. Equilibrium phase's nature was identified at four temperatures for our two alloys. Equilibrium phase fractions and chemical compositions were determined at 900°C. Thanks to these equilibrium results, we tried to understand non-equilibrium microstructure observed after different thermal history (DTA cycles, isothermal treatment followed by quench, reception state) and identify DTA events in a coherent way. The main role of grain boundaries in phase precipitation was pointed out and need to be further described.

Further experiments should be done into the high temperature domain to determine the limits of the austenite containing phase fields.

REFERENCES

1) G. Frommeyer, E. J. Drewes and B. Engl: *Rev. Metall.* (*Paris*), **10** (2000), 1245.
2) U. R. Kattner and B. P. Burton: Phase Diagrams of Binary Iron Alloys, ed. by H. Okamoto, ASM Int., Materials Park, OH, USA, (1993), 12.
3) M. Palm and G. Inden: *Intermetallics*, **3** (1995), 443.
4) K. H. Han: *Mater. Sci. Eng.*, **197** (1995), 223.
5) Y. Kimura, K. Handa, K. Hayashi and Y. Mishima: *Intermetallics*, **12** (2004), 607.
6) W. S. Yang, B. T. Wu, K. H. Hwang, J. G. Byrne and C. M. Wan: *Scr. Metall. Mater.*, **24** (1990), 1221.
7) M. C. Li, H. Chang, P. W. Kao and D. Gan: *Mater. Chem. Phys.*, **59** (1999), 96.
8) H. Y. Chu, F. R. Chen and T. B. Wu: *Scr. Metall. Mater.*, **33** (1995), 1269.
9) W. B. Lee, F. R. Chen, S. K. Chen, G. B. Olson and C. M. Wan: *Acta Metall. Mater.*, **43** (1995), 21.
10) H. Y. Chu, F. R. Chen and T. B. Wu: *Matall. Lett.*, **30** (1997), 369.
11) W. C. Cheng, C. F. Liu and Y. F. Lai: *Scr. Mater.*, **48** (2003), 295.
12) K. Ishida, H. Ohtani, N. Satoh, R. Kainuma and T. Nishizawa: *ISIJ Int.*, **30** (1990), 680.
13) W. C. Cheng and H. S. Lin: *Mater. Sci. Eng.*, **323** (2002), 426.
14) K. H. Hwang, C. M. Wan and J. G. Byrne: *Mater. Sci. Eng.*, **132** (1991), 161.
15) J. W. Martin, R. D. Doherty and B. Cantor: Stability of Microstructure in Metallic Systems, 2nd ed., Cambridge Solid State Science Series, Cambridge University Press, Cambridge, UK, (1997), 251.
16) A. A. Coelho, M. Imaizumi, B. Laks, A. A. Araújo, M. A. Mota, S. Gama, M. Jafelicci, L. C. Laudemir and C. Varanda: *J. Magn. Magn. Mater.*, **272**–**276** (2004), 769.
17) W. Zarek, E. Talik, J. Heimann, M. Kulpa, A. Winiarska and M. Neumann: *J. All. Comp.*, **297** (2000), 53.
18) W. K. Choo, J. H. Kim and J. C. Yoon: *Acta Mater.*, **45** (1997), 4877.
19) J. W. Lee and T. F. Liu: *Mater. Chem. Phys.*, **69** (2001) 192.